Environmental Fluid Mechanics manuscript No.
(will be inserted by the editor)

A field study of interfacial friction and entrainment in a microtidal salt-wedge estuary

Nino Krvavica · Vanja Travaš · Nevenka Ožanić

DOI: 10.1007/s10652-016-9480-1

Abstract The interfacial friction and entrainment were investigated in a microtidal salt-wedge estuary. A detailed sampling campaign was conducted in the Rječina River estuary in Croatia from January 2014 to June 2015. The observed vertical profiles of salinity s and temperature T confirmed the presence of a highly stratified estuary, represented by an upper layer of freshwater separated from a lower salt-wedge by a sharp density interface. The entrainment rate E across the interface was estimated by a two-layer box-model, based on the observed freshwater flow rate Q and layer-averaged salinity. Interfacial friction factor λ_i was estimated by fitting the results of a numerical model to the observed interface depths. For this purpose we applied a numerical two-layer shallow water model extended to account for irregular non-prismatic cross sections of the channel. We found that in microtidal conditions, the strength of the stratification is reduced with increasing Q. Furthermore, we found that as Q increases, so does the shear velocity, the interfacial friction factor and the vertical mixing across the interface. More detail analysis showed that E may be parametrized by bulk non-dimensional parameters, in particular, a combination of bulk Richardson number Ri and average friction factor λ, which accounts for the channel bed friction and the interfacial friction. On the other hand, λ_i can be linked to a combination of Reynolds number Re and bulk Richardson Ri. Contrary to previous studies, we showed that in field conditions, λ_i may increase with Re.

Keywords Estuaries · Stratified flow · Salt-wedge · Two-layer model · Interfacial friction · Entrainment

1 Introduction

Salt-wedge estuaries, develop at the mouths of coastal rivers where the ratio of river to tidal flow is high enough to maintain a strong density stratification [10]. These types of estuaries are characterized by an upper layer of freshwater flowing downstream towards the

N. Krvavica · V.Travaš · N. Ožanić
Faculty of Civil Engineering, University of Rijeka
Radmile Matejcic 3, 51000 Rijeka, Croatia
Tel.: +385-51-265932
E-mail: nino.krvavica@uniri.hr

river mouth over a lower layer of heavier saltwater advancing upstream. The shape of a salt-wedge is influenced by the channel geometry and flow parameters, such as the velocity, depth, and fluid density. For constant sea level and river flow rate, an arrested salt-wedge may be established, where only the upper layer is active. However, steady states are rarely present in the field due to tidal dynamics [15].

Highly stratified estuarine conditions are observed in many estuaries worldwide. Most of the research found in the literature is focused on macrotidal salt-wedge estuaries, such as the Fraser, Merrimack and Snohomish River [28, 35, 46], where a strong stratification is maintained by high river flow rates which dampen the intensity of vertical mixing caused by tidal dynamics. However, in microtidal seas, which are common in the Mediterranean region, estuaries are highly stratified even for relatively low river flow rates. A typical examples of such estuaries are the Ebro River in Spain [20] or Neretva River in Croatia [27]. Unfortunately, very few studies of physical processes in microtidal estuarine environments can be found in the literature. Understanding salt-wedge characteristics is important in many engineering and environmental problems, such as predicting the impact of channel dredging or widening in coastal areas, planning and managing structural measures for saltwater intrusion or freshwater withdrawal from estuaries, and studying pollutant or sediment transport in stratified environments.

The first mathematical models for predicting the shape of a salt-wedge were developed by Schijf and Schönfeld [37] and Farmer and Morgan [11]. These models are based on the shallow water theory for two layers, and they incorporate several simplifications, such as a rectangular cross section, a horizontal channel bed, no wall or bed shear stress, no mixing, and a sharp density interface. In subsequent years, two-layer models were improved by considering channel geometry with variable breadth and bed slope [4], wall and bed shear stress [9], lower layer dynamics including entrainment [3] and interfacial mixing [17]. These improved models were eventually extended to create a three-layer model by including the interfacial layer [19, 38]. A good model for salt-wedge prediction should only need the freshwater flow rate Q, fluid density ρ, and total depth at the mouth H as input parameters. The main issue in the two-layer theory, however, is the parametrisation of the interfacial friction factor λ_i and the entrainment rate E.

Interfacial processes in a stratified flow are governed by the stability of internal waves [1]. For stable flow conditions, the interface between the layers is smooth and laminar. When the freshwater velocity increases, internal waves form at the interface, which increases the apparent roughness. If the velocity exceeds a certain value, stability is compromised and the internal waves brake and generate mixing, causing an interfacial layer to develop. Once a stable interfacial layer is established, internal waves stabilize and turbulent mixing is reduced. The interfacial shear stress τ_{int} varies according to the stage of the interfacial layer development and is influenced by the turbulence generated at the interface and at the channel bed [1]. The quadratic friction law defines

$$\tau_{int} = \lambda_i \rho \Delta u^2, \tag{1}$$

where $\Delta u = u_1 - u_2$ is the difference between the upper and lower layer velocities.

A very comprehensive review of λ_i is given in [1, 2, 22]. Numerous attempts to combine data from different sources and create a unified friction law are documented in [2, 22, 43, 44]. Unfortunately, the data scattering in those studies is too extensive to allow any of the friction models to accurately predict the shape of salt-wedges in field conditions. Under ideal laboratory conditions, the dynamics of a salt-wedge appears to be governed by two non-dimensional parameters, freshwater Reynolds number Re and densimetric Froude number

Fd [2], which are defined as

$$Re = \frac{u_1 R_1}{\nu}, \tag{2}$$

$$Fd = \frac{u_1}{\sqrt{g(1-r)h_1}}, \tag{3}$$

where u_1, h_1 and R_1 are velocity, depth and hydraulic radius for the upper layer, respectively; ν is freshwater kinematic viscosity; g is gravity acceleration, and $r = \rho_1/\rho_2$ is the ratio of upper layer density ρ_1 to the lower layer density ρ_2. Field studies are scarce, however, and they are usually limited to only a few usable data sets. Furthermore, some of the published results, are limited by insufficient information for a more extensive common analysis [2]. The main difficulties in obtaining a relevant set of interfacial friction factors λ_i from the field, can be identified in: a) the time-dependent flow conditions of natural estuaries, b) the inability to conduct measurements under systematic variation of the main flow parameters, and c) the high sensitivity of λ_i to the slope of the interface, which can sometimes be difficult to accurately measure in the field if the interfacial thickness varies along the wedge.

In recent years, many authors who studied stratified flow using shallow water models showed that the numerical solutions are sensitive to λ_i, which is very difficult to determine a priori [19, 34]. Hence, more field measurements are needed to validate existing friction equations [14,38]. Unfortunately, since Arita and Jirka in 1987 [2,3], who proposed a semi-empirical equation for λ_i as a function of Re and bulk Richardson number Ri, no attempts were made to derive a suitable parametrisation of interfacial friction factor in salt-wedge estuaries based on known bulk parameters, and no additional data sets from the field were provided to re-evaluate the existing equations. Bulk Richardson number is defined as

$$Ri = \frac{g(1-r)h_1}{\Delta u^2}. \tag{4}$$

Another important process in salt-wedge estuaries is the interfacial mixing, which can be classified either as entrainment or turbulent mixing [6]. When the interfacial layer is in a subcritical state entrainment mixing takes place. The interfacial layer becomes critical when $Ri_\delta < 1.2$, where Ri_δ is a shear layer Richardson number defined as [18]:

$$Ri_\delta = \frac{g(1-r)\delta_u}{\Delta u^2}. \tag{5}$$

where δ_u is shear layer thickness. If one of the layers is non-turbulent, the one-way process occurs from a non-turbulent to a turbulent layer (*pure entrainment*). If both layers are turbulent then a two-way process occurs, usually called *net entrainment*; it describes the difference between the rate of upward and downward entrainment. Turbulent mixing occurs when the interfacial layer is in a critical or supercritical state, with equal amounts of fluid being exchanged between the layers [17].

A good review of entrainment rates E in stratified flows can be found in [8, 12]. Earlier studies mainly focused on the entrainment parametrization, that is, the relationship between the entrainment rate $E = w_e/\Delta u$, where w_e is the entrainment velocity, and governing non-dimensional parameters, such as Fd or Ri. Depending on the type of stratified flow, the shear entrainment rate $E_* = w_e/u_*$ is sometimes used instead of E, and shear Richardson number $Ri_* = g(1-r)h_1/u_*^2$ is used instead of Ri, where $u_* = \sqrt{(\tau/\rho)}$ is the shear velocity. Based on numerous experiments it is considered that E reduces with increasing Ri [8, 12].

Recent studies are more focused on the fundamental understanding of the mechanism of the turbulent mixing and the complex interaction between the interfacial shear, mixing

and stratification [16, 35, 41]. The strength of stratification is usually quantified by a Brünt-Väisälä or buoyancy frequency N, which is defined as

$$N^2 = -\frac{g}{\bar{\rho}} \frac{\partial \rho(z)}{\partial z}, \tag{6}$$

where $\bar{\rho}$ is mean density, and $\rho(z)$ is density at depth z. The shear S can be expressed in the same units (s^{-2}) as

$$S = \frac{\partial u(z)}{\partial z}. \tag{7}$$

Shear and stratification influence turbulent mixing in opposite ways; stronger stratification dampens the turbulent energy, while shear stress initiate the production of turbulent energy and increases the mixing [40]. Thus, the ratio of N^2 to S^2 is expressed by a gradient Richardson number as

$$Ri_g = \frac{N^2}{S^2} = -\frac{\frac{g}{\bar{\rho}} \frac{\partial \rho(z)}{\partial z}}{\left(\frac{\partial U(z)}{\partial z}\right)^2}. \tag{8}$$

Gradient Richardson number provides a more physical interpretation of the interfacial dynamics; it represents a ratio of stabilizing to destabilizing forces and indicates whether the flow is prone to shear instabilities [40]. It is considered that as Ri_g increases the effects of stratification becomes more prominent and the turbulent mixing should be reduced. Under the assumption that the interfacial thickness δ_i is equal to the shear layer thickness δ_u, which is valid for high Re, Richardson gradient number can be approximated as [28]:

$$Ri_g \approx Ri'_g = \frac{g(1-r)\delta_i}{\Delta u^2}. \tag{9}$$

Numerous studies of interfacial mixing in stratified flows provide valuable insight, but the exact mechanisms are not yet completely understood, and both qualitative and quantitative discrepancies are present when the results are combined [12, 19]. While current trends in the literature, which employ 3D models and different turbulence closure schemes, are crucial in understanding the mechanisms of turbulent mixing, in many numerical models, especially layered shallow water models, the interfacial friction and entrainment are parametrized based on bulk nondimensional parameters. Although both these interfacial processes have been thoroughly examined in laboratory experiments, field observations are scarce and we are still far from a reliable entrainment law for salt-wedge estuaries. Considering that the dynamic situation at the interface can only be qualitatively similar to field conditions, and quite different results should be expected in a quantitative sense [21], many authors emphasized the importance of validating the existing parametrizations with field observations [12, 14, 19, 28, 34, 38].

The aim of the current study is twofold: first, to examine the governing interfacial processes in a microtidal salt-wedge estuary, which are rarely found in the literature; and second, to re-evaluate the existing interfacial friction and entrainment equations, and examine how accurately they predict the salt-wedge dynamics in the Rječina River estuary. To do so, we used a simple box model and developed an improved shallow water model for two-layer flow in arrested salt-wedge estuaries. Next, we validated the performance of the numerical model in computing the arrested salt-wedge shape by comparing the solutions against field observation. The interfacial friction coefficient was fitted to field observations, as well as calculated from existing friction equations. Finally, we discuss the correlation of E and λ_i with different parameters, and examine how well they agree with existing equations.

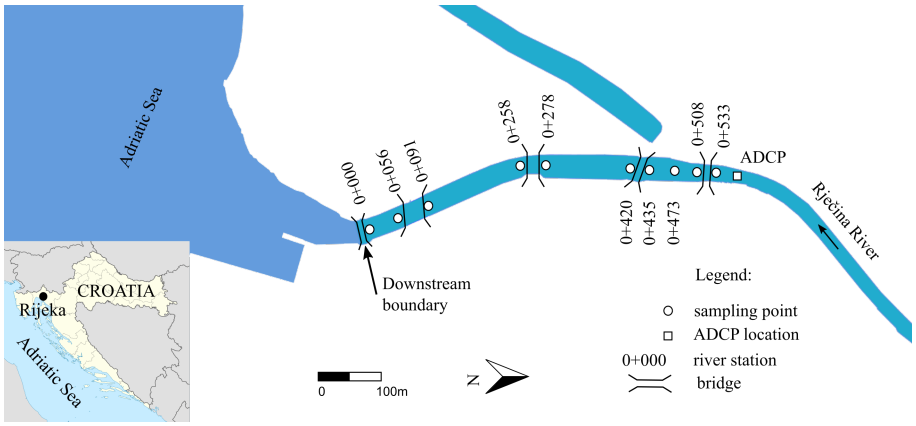

Fig. 1 Location map of the Rječina River estuary with sampling points

2 Methodology

2.1 Site description

Rječina River is a short karst river, located in the northern coastal part of Croatia, in the city centre of Rijeka (Fig. 1). The river is characterized by strong seasonal oscillations, with maximum flow rates in winter months and minimum rates in summer months. Its mean annual flow rate is $Q = 10.4$ m^3 s^{-1} (1999-2011). Inter-daily oscillations are also common in the lower reaches of the Rječina River due to periodic operating conditions of the hydropower plant Rijeka.

Rječina River estuary is located at 45°19' N latitude and 14°27' E longitude (Fig. 1). The estuary is characterized by a short intrusion length and steep bottom slope; the maximum intrusion length is about 1 km, the maximum depth near the mouth is $H = 4.2$ m, and the average bottom slope is $I = 0.4\%$ (Fig. 2). In the upper reaches of the estuary, the channel cross sections are narrow with vertical walls, while cross sections are wider with mildly sloped sides and a natural bed in the middle and lower reaches (Fig. 3). Tidal oscillations are semi-diurnal with a mean daily amplitude of approximately 30 cm. All of these characteristics make the Rječina river estuary a very favourable site for salt-wedge field observation. Steady flow conditions are easily achieved there because of the controlled and uniform freshwater flow rate Q, very small tidal oscillations and relatively short intrusion length [25].

The field sampling campaign was carried out in the Rječina River estuary during numerous occasions from January 2014 until June 2015 for different hydrological conditions. The observations covered the sea levels from -0.07 to $+0.75$ m above sea level (asl), and freshwater flow rates from $Q = 2.0$ to 31.3 m^3 s^{-1}. Up to 10 sampling points were selected, with most of them located at five bridges spanning the Rječina River estuary (Fig. 1). Vertical profiles of salinity s and temperature T were measured using a Schlumberger CTD diver, and freshwater flow rates Q were measured upstream from the tip of the salt-wedge by Teledyne Stream Pro ADCP. Densities in each layer $\rho_{1,2}$ were calculated from s-T profiles using well known empirical equations [13]. Only the observations obtained for stationary flow conditions, and minimal influence of wind or waves, were considered. After the selection, a total of 22 out of 30 data sets were chosen for further analysis of interfacial processes.

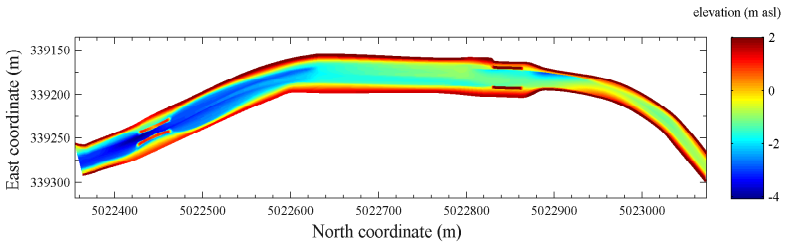

Fig. 2 Bathymetry of the Rječina River estuary

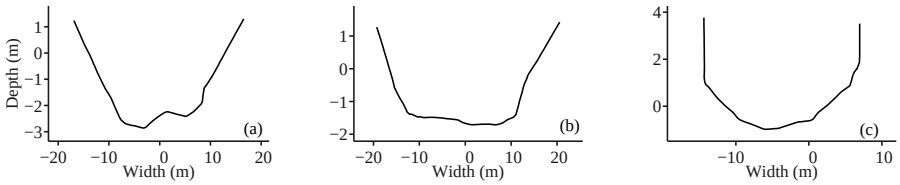

Fig. 3 Characteristic cross-section profiles for a) lower reaches of the estuary (0+150), b) middle of the estuary (0+325), c) upper reaches of the estuary (0+650)

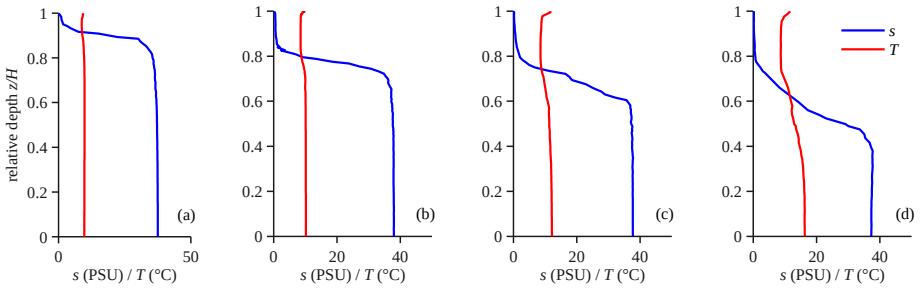

Fig. 4 Vertical profiles of salinity s and temperature T observed in the Rječina River estuary at station (0+091), for freshwater flow rate a) $Q = 2.8$ m^3 s^{-1}, b) $Q = 13.4$ m^3 s^{-1}, c) $Q = 16.8$ m^3 s^{-1}, and d) $Q = 29.8$ m^3 s^{-1}

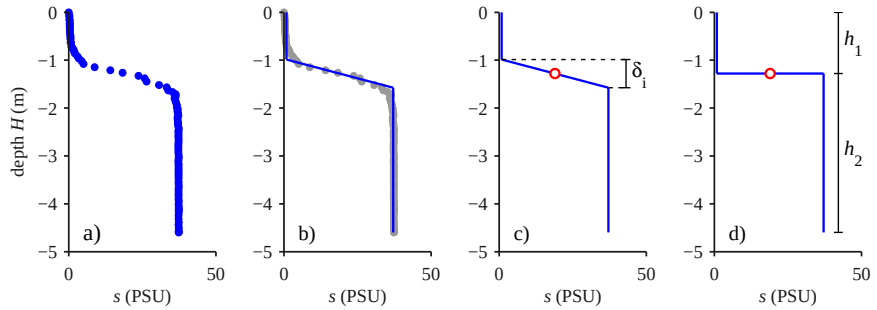

Fig. 5 Vertical profile of salinity s for flow rate $Q = 17.2$ m^3 s^{-1}: a) observed salinity profile, b) linearised salinity profile, c) interface thickness δ_i, d) approximated salinity profile and interface depth (red circle) for the numerical model

Figure 4 shows four characteristic vertical $s-T$ profiles, observed during different Q at the Rječina River estuary. Vertical profiles are consistent along the salt-wedge for steady flow. As expected, the interface depth grows with Q, but the influence of the upper layer flow on the interfacial layer thickness is also notable. For lower flow rates, a sharp gradient is preserved (Fig. 4a,b), as the flow rate increases above $Q > 14$ m^3 s^{-1}, the interfacial layer becomes more diffusive and its thickness grows (Fig. 4c). For very high flow rates ($Q = 29.8$ m^3 s^{-1}), the interface is characterized by a well-defined mixed layer (Fig. 4d).

Figure 5 shows the observed salinity profile and the method for estimating the interfacial layer thickness δ_i. First, we computed an average salinity gradient inside the interfacial layer,

$$\frac{\Delta S}{\delta_i} = \frac{S_{25\%} - S_{75\%}}{z_{S25\%} - z_{S75\%}}, \tag{10}$$

where $S_{25\%} = 0.25\max(s)$ and $S_{75\%} = 0.75\max(s)$, $z_{S25\%}$ and $z_{S25\%}$ are the corresponding vertical coordinates. Next, we computed the average salinity over the upper layer $S_1 = \text{mean}(s(z) < 0.05\max(s))$ and lower layer $S_2 = \text{mean}(s(z) > 0.95\max(s))$, hence $\Delta S = S_2 - S_1$. The points where these three lines intersect are the upper and lower boundary of the interfacial layer, which defines the interfacial layer thickness δ_i. The midpoint of the interfacial layer is considered to be the interface depth (red dot in Fig. 5c,d). Finally, based on the interface depth, we may compute the upper h_1 and lower h_2 layer height for a two-layer approximation. We found that, for most cases, the interface depth located in the middle of the interfacial layer is very close to the midpoint in salinity and to the maximum salinity gradient, which may also be used to defined the interface depth.

2.2 Two-layer box model

A simple two-layer box model was applied to compute the interfacial mixing from the observed values. This model is based on Knudsens hydrographical theorem for conservation of volume and salt, which is appropriate for strongly stratified estuaries, steady flow conditions, and negligible tidal effects [10]. Given that the Rječina River estuary is relatively short and the channel geometry is fairly uniform (Fig. 2), we computed the along-wedge average values of vertical exchange between the upper and lower layer. Hence, the entire length of the salt-wedge was considered a single box, where the upstream boundary (a) represent the tip of the salt-wedge, and the downstream boundary (b) is located near the salt-wedge exit region (Fig. 6). Under the assumption of constant vertical profiles of velocity $u_1(z) = U_1$, $u_2(z) = U_2$, and salinity $s_1(z) = S_1$, $s_2(z) = S_2$, continuity equations for water and salt in the upper and lower layer are written as follows:

$$Q_1^{(a)} + Q_{21} = Q_{12} + Q_1^{(b)} \tag{11}$$

$$Q_2^{(a)} + Q_{21} = Q_{12} + Q_2^{(b)} \tag{12}$$

$$Q_1^{(a)} S_1^{(a)} + Q_{21}\overline{S_2} = Q_{12}\overline{S_1} + Q_1^{(b)} S_1^{(b)} \tag{13}$$

$$Q_2^{(a)} S_2^{(a)} + Q_{21}\overline{S_2} = Q_{12}\overline{S_1} + Q_2^{(b)} S_2^{(b)} \tag{14}$$

where Q_i is the horizontal flow rate; Q_{ij} is the average vertical flow rate inside the box; S_i is the salinity; $\overline{S_i}$ is the average salinity inside the box; and $i = 1,2$ denotes the upper and lower layer, respectively.

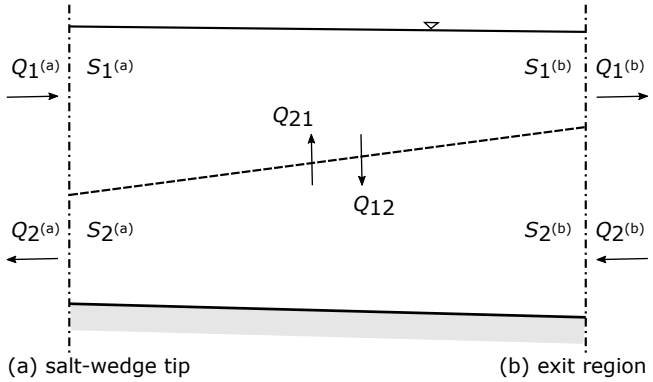

Fig. 6 Scheme of a two-layer box model for estimating the entrainment

For the upstream boundary conditions, the following values were used: $Q_1^{(a)}$ equals the observed freshwater flow rate Q; salinity in the upper layer is $S_1^{(a)} = 0$; and $S_2^{(a)}$ is equal to the observed value at the most upstream profile. At the downstream boundary, the observed values were used for the upper $S_1^{(b)}$ and lower $S_2^{(b)}$ layer salinities. Finally, the horizontal flow rates $Q_1^{(b)}$ and $Q_2^{(b)}$, as well as downward Q_{12} and upward Q_{21} flow rates, were calculated for both layers by solving the set of equations 11-14.

The vertical volume fluxes w_{12} and w_{21} were estimated by dividing the downward and upward flow rates Q_{12} and Q_{21} by the surface area A_{int}, separating the two layers through which the vertical transport takes place, $w_{12} = Q_{12}/A_{int}$ and $w_{21} = Q_{21}/A_{int}$. Finally, the entrainment velocity $w_e = w_{21} - w_{12}$ was obtained from the difference between the upward w_{21} and downward w_{12} volume flux.

2.3 Numerical model for two-layer shallow water flow

Schijf and Schönfeld [37] based their two-layer theory on the assumption of two immiscible layers separated by a sharp interface, hydrostatic pressure, constant velocity and density profile for each layer, valid Boussinesq approximation and rectangular cross-section. Because only a small amount of mixing occurs in salt-wedges (usually net entrainment from lower to upper layer), it is usually disregarded in two-layer models. Although the influence of entrainment mixing on average fluid densities along the wedge is small, its effect on the lower layer dynamics can be noticeable though, especially for long estuaries usually encountered in the field [2].

Grubert [17] extended the model [37] by including the entrainment velocity in both continuity and momentum equations. We further extend this scheme by considering a channel with irregular non-prismatic cross-sections. The proposed model is defined by the continuity equations for the upper and lower layer, as follows

$$\frac{\partial A_1}{\partial t} + \frac{\partial Q_1}{\partial x} = w_e \sigma_3, \tag{15}$$

$$\frac{\partial A_2}{\partial t} + \frac{\partial Q_2}{\partial x} = -w_e \sigma_3, \tag{16}$$

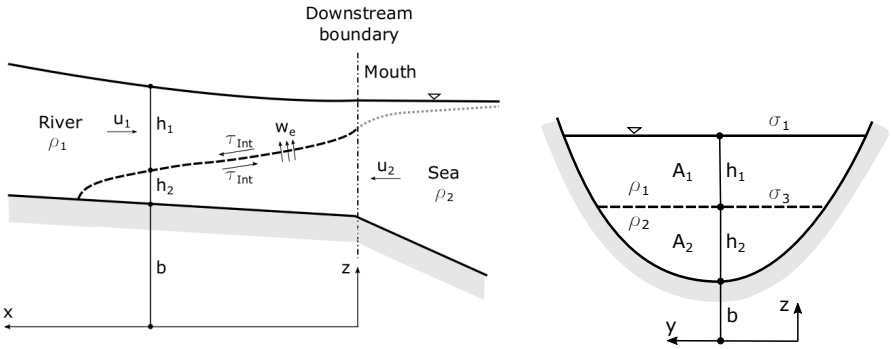

Fig. 7 Longitudinal and cross section scheme for a two-layer numerical model

and the momentum equations for the upper and lower layer,

$$\frac{\partial Q_1}{\partial t}+\frac{\partial}{\partial x}\left(\frac{Q_1^2}{A_1}\right)+gA_1\frac{\partial}{\partial x}\left(b+h_2+h_1\right)=\frac{\tau_{int}}{\rho_1}\sigma_3+\frac{\tau_w}{\rho_1}(O_1-\sigma_3)+w_e u_1\sigma_3, \tag{17}$$

$$\frac{\partial Q_2}{\partial t}+\frac{\partial}{\partial x}\left(\frac{Q_2^2}{A_2}\right)+gA_2\frac{\partial}{\partial x}\left(b+h_2+rh_1\right)=-\frac{\tau_{int}}{\rho_2}\sigma_3+\frac{\tau_b}{\rho_2}O_2-w_e u_2\sigma_3, \tag{18}$$

where Q_i is the flow rate; A_i, cross section area; b, channel bed height; h_i, water depth; ρ_i, density; σ_3, channel breadth at the interface; O_i, wetted perimeter; w_e, entrainment velocity; and u_i, horizontal velocity; and index $i=1,2$ denotes the upper and lower layers, respectively. Interfacial τ_{int}, wall τ_w, and bed τ_b shear stress are defined as follows:

$$\tau_{int}=-\rho_1\lambda_i|u_1-u_2|(u_1-u_2), \tag{19}$$

$$\tau_w=-\rho_1\lambda_w|u_1|u_1, \tag{20}$$

$$\tau_b=-\rho_2\lambda_b|u_2|u_2, \tag{21}$$

where λ_i, λ_w, and λ_b are interfacial, wall, and bed friction factor, respectively.

For steady flow conditions, the system of Eqs. (15)-(18) takes the following form:

$$\frac{\mathrm{d}Q_1}{\mathrm{d}x}=w_e\sigma_3, \tag{22}$$

$$\frac{\mathrm{d}Q_2}{\mathrm{d}x}=-w_e\sigma_3, \tag{23}$$

and the momentum equations:

$$\frac{\mathrm{d}}{\mathrm{d}x}\left(\frac{Q_1^2}{2gA_1^2}+b+h_2+h_1\right)=\frac{\tau_{int}}{\rho_1 gA_1}\sigma_3+\frac{\tau_w}{\rho_1 gA_1}(O_1-\sigma_3)+\frac{w_e u_1}{gA_1}\sigma_3, \tag{24}$$

$$\frac{\mathrm{d}}{\mathrm{d}x}\left(\frac{Q_2^2}{2gA_2^2}+b+h_2+rh_1\right)=-\frac{\tau_{int}}{\rho_2 gA_2}\sigma_3+\frac{\tau_b}{\rho_2 gA_2}O_2-\frac{w_e u_2}{gA_2}\sigma_3. \tag{25}$$

When a prismatic channel with a rectangular cross section is considered and the entrainment is disregarded, Eqs. (22) and (23) can be incorporated in Eqs. (24) and (25). Furthermore, Eq. (25) can be subtracted from Eq. (24), and a single ordinary differential equation (ODE) is obtained describing the slope of the interface from the mouth upstream:

$$\frac{\mathrm{d}h_1}{\mathrm{d}x} = \frac{Fd^2}{Fd^2-1}\left[\lambda_i\left(1+\frac{h_1}{h_2}\right)-2\lambda_w\frac{h_1}{\sigma}\right]. \tag{26}$$

Equation (26) can be further simplified by neglecting the wall friction λ_w and assuming a horizontal channel bed. In this case, Eq. (26) can be integrated over depth, which leads to a well-known analytical expression [37] for the length L of a salt-wedge normalized by the total water depth H:

$$\frac{L}{H} = \frac{1}{4\lambda_i}\left(3F_0^{2/3}-\frac{6}{5}F_0^{4/3}-2+\frac{1}{5}F_0^{-2}\right), \tag{27}$$

where F_0 is the densimetric Froude number just upstream from the tip of a salt-wedge. Obviously, Eq. (26) or (27) are much more attractive than the system of Eqs. (22)-(25); the interfacial friction factor λ_i can be directly obtained by knowing the normalized length of the wedge L/H or the interface slope $\mathrm{d}h_1/\mathrm{d}x$. Most of the documented studies in which λ_i was calculated from the measurements were based exactly on such, or very similar, equations [9, 39, 43].

Considering that the salt-wedge profile in the Rječina River estuary is highly sensitive to λ_i [24], we took a different approach. By accounting for irregular non-prismatic cross sections of the Rječina River estuary, the system of Eqs. (22)-(25) was solved numerically using the implicit trapezoidal method rule [42]. The model was defined by r computed from the observed layer-averaged densities and w_e obtained from the box model (Eq. 11-14). The downstream boundary condition was forced by Q, and H and h_1 at the mouth. The interfacial friction factor was assumed to be constant along the wedge and was systematically varied until the best fit between the numerical results and observed interfacial depths was achieved. In the process of finding the best fit, λ_i was varied over the range $10^{-5}-10^{-2}$ by the increment of 10^{-5}. The best fit was determined by the visual inspection and by the smallest root mean square error, defined as

$$RMSE = \sqrt{\frac{1}{n}\sum_{i=1}^{n}\left(y_{obs,i}-y_{mod,i}\right)^2}, \tag{28}$$

where n is the total number of observations along the wedge, y_{obs} is the observed depth of the interface, and y_{mod} is the numerical solution for the interface depth. This approach allowed us to more accurately account for the variable channel geometry, lower layer dynamics, bed shear stress, entrainment and in the end to obtain more accurate results.

3 Results

The observed values from sampling campaigns in the Rječina River estuary are presented in Table 1. The freshwater flow rate Q, measured by ADCP just upstream from the tip of the salt wedge, ranged from 2.0 m^3 s^{-1} to 31.3 m^3 s^{-1}, and the sea levels, measured by a water gauge at the mouth, ranged from -0.07 m to +0.75 m asl. The observed s-T profiles where linearised, as shown in Fig. 5, to obtain layer-averaged values, which were

then used to compute layer-averaged densities. The reduced gravity $g(1-r)$ ranged from 0.235 to 0.271. The interface thickness δ_i was obtained from salinity profiles using Eq. (10), as illustrated in Fig. 5, and averaged along the wedge; it ranged from 0.19 to 0.76 m. Upper layer depth h_1 and lower layer depth h_2 were computed as a vertical distance between the water surface and the interface, and between the interface and channel bed, respectively, and then averaged along the wedge. The interface depth was assumed to be located in the middle of the interfacial layer δ_i, as illustrated in Fig. 5. Maximum squared buoyancy frequency N^2 (Eq. 6), as a measure of the stratification strength, was computed from vertical density profiles and then averaged along the wedge. N^2 in the Rječina River estuary shows values ranging from 0.4 s^{-2} to 1.7 s^{-2}, suggesting the presence of a highly stratified water column under all hydrological conditions.

The entrainment velocity w_e was estimated by the box model (Eq. 11-14) and it also represents an along wedge average value. The upward water flux w_{21} was a few times to a few orders of magnitude larger than the downward water flux w_{12}, and the corresponding entrainment velocity ranged from $w_e = 1.0 \times 10^{-5}$ to 2.8×10^{-4} m s^{-1}. The box model indicated that lower layer horizontal flow rates Q_2 ranged from -0.1 to -1.0 m^3 s^{-1}, directed upstream as a result of mixing processes. The lower layer circulation varied from 3% to 15% of the freshwater flow rate Q. Similar values of w_e were found at the Ebro River estuary in Spain [20] and the Jadro River estuary in Croatia [26], both microtidal salt-wedges, while the values in macrotidal salt-wedge estuaries, in particular the Duwamish River [31] and the Fraser River [28], are one order of magnitude higher, probably because of stronger tidal mixing.

The steady flow profiles of the upper and lower layer were calculated by numerically solving the two-layer shallow water system of Eqs. (22)-(25) for different boundary conditions. The calculation started at the downstream boundary positioned at the last bridge near the river mouth (Fig. 1). At the boundary, the observed flow rates in each layer, Q_1 and Q_2, upper layer depth h_1, and water depth H were set. Additionally, the model was defined by$r$ computed from densities observed in the field. The entrainment velocity was assumed constant along the wedge, and computed by the box model for each observation. The wall and bed friction factors were calculated from Manning's roughness factor $n = 0.025$ s $m^{-1/3}$ (for channels with gravel bottom and concrete/stone sides). Finally, the numerical solutions were fitted to the observed interface depths by systematically varying λ_i as described earlier. The interfacial friction factor was assumed to be constant along the wedge, and the best fit was determined by the visual inspection and by the smallest *RMSE* (Eq. 28).

The numerical solution of interface depths along the wedge are shown in Fig. 8, for several different freshwater flow rates and sea levels. Overall, the proposed model agreement with the field observations is satisfactory when λ_i is fitted (mean $RMSE = 0.11$ m). The length and shape of the arrested salt-wedge seems to be influenced by both sea level and freshwater flow rate. For constant Q, salt-wedge length increases with sea level, similarly, for constant sea level, salt-wedge intrudes upstream as Q decreases. For example, salt-wedge length was shorter for $Q = 10$ m^3 s^{-1} than for $Q = 17.9$ m^3 s^{-1}, because of a higher sea level in the latter case (Fig. 8). However, the salt-wedge length depends also on the channel geometry, as stepper slopes or sills may limit the salt-wedge from advancing further upstream.

We also show the numerical solutions obtained by a simpler single ODE model (Eq. 26) in Fig. 8 to illustrate the differences between a numerical model, which accounts for the irregular geometry and an ODE, which neglects the influence of the channel bottom slope and variable cross sections. Clearly, the proposed numerical model (Eq. 22-25) is a significant improvement over the ODE; it seems that the ODE generally underestimates the slope of the

Table 1 Observed values in the Rječina River estuary. Freshwater flow rate Q measured upstream from the salt-wedge by ADCP, *sea level* measured by a water gauge at the mouth, $g = 9.81$ m s^{-2}, layer-averaged density ratio $r = \rho_1/\rho_2$ computed from the observed density profiles, freshwater viscosity ν computed from the measured density and temperature profiles, upper and lower layer depth h_1 and h_2 (see Fig. 5d), interfacial thickness δ_i (see Fig. 5c), maximum squared buoyancy frequency N^2 (Eq. 6), and entrainment velocity w_e obtained from the box model (Eq. 11-14). All parameters in the columns 5 - 10 are averaged along the wedge.

nr.	Q (m^3 s^{-1})	*sea level* (m asl)	$g(1-r)$ (m s^{-2})	$10^6\nu$ (m^2 s^{-1})	h_1 (m)	h_2 (m)	δ_i (m)	N^2 (s^{-2})	$10^5 w_e$ (m s^{-1})
1	2.0	0.4	0.257	0.96	0.40	2.54	0.39	0.71	0.99
2	2.8	0.25	0.268	1.34	0.49	2.30	0.19	1.71	0.98
3	4.8	-0.04	0.237	1.18	0.82	1.68	0.33	0.68	2.79
4	4.8	0.1	0.239	1.26	0.75	1.90	0.32	0.77	1.51
5	5.1	0.04	0.253	1.27	0.79	1.79	0.30	0.71	2.24
6	5.3	-0.07	0.245	1.26	0.82	1.65	0.24	0.94	2.69
7	5.7	0.03	0.235	1.19	0.89	1.69	0.43	0.57	3.87
8	7.8	0.6	0.266	1.25	0.97	2.17	0.54	0.52	4.64
9	10.0	0.12	0.249	1.27	1.44	1.22	0.22	0.98	2.70
10	10.0	0.18	0.244	1.23	1.30	1.43	0.23	0.81	5.74
11	11.3	0.14	0.254	1.34	1.48	1.21	0.34	0.87	3.90
12	11.4	0.6	0.264	1.34	1.36	1.79	0.26	1.12	4.00
13	11.5	-0.01	0.255	1.23	1.51	1.04	0.31	0.89	4.53
14	12.3	-0.04	0.251	1.34	1.53	0.98	0.25	0.98	4.37
15	13.4	0.25	0.271	1.35	1.67	1.13	0.36	0.62	6.69
16	14.1	0.5	0.265	1.30	1.52	1.53	0.31	0.95	7.37
17	16.3	0.16	0.248	1.30	1.80	0.92	0.52	0.53	9.42
18	16.8	0.25	0.268	1.35	1.85	0.96	0.76	0.72	7.82
19	17.2	0.45	0.264	1.34	1.86	1.14	0.48	0.60	8.36
20	17.9	0.75	0.265	1.34	1.66	1.64	0.29	0.84	4.98
21	29.8	0.15	0.258	1.34	2.39	0.36	0.62	0.38	25.88
22	31.3	0.35	0.251	1.33	2.53	0.41	0.65	0.39	27.54

interface for the same λ_i, and more importantly, the slope of the interface is too idealized, i.e., the ODE solutions can not compute the realistic changes in the interface slope due to bed slope or channel width variability. When the analytical model (Eq. 27) was used, the predicted intrusion lengths exceeded the observed values by several orders of magnitude. This is to be expected, however, because the analytical model not only neglects the influence of the bottom slope and variable cross section, but it also assumes that the channel bed is horizontal and that the total depth is equal to the one at the mouth. The same unreliability of the analytical model when applied to natural estuarine channels was observed in [34].

When existing interfacial friction laws [3,9,43] were applied to calculate λ_i, they either overestimated or underestimated the length of the salt-wedge. Dermissis and Partheniades [9] found that correlating λ_i with either Re, Fd, or Keulegan number $K = ReFd^2$ resulted in wide scattering of the observed data. They proposed that scattering may be minimized if λ_i is linked to $ReFr^2$, with additional independent parameter $\Delta\rho/\rho$. Here, Fr denotes the standard Froude number $Fr = u_1/\sqrt{gh_1}$. Unfortunately, in [9] no equation was given, only a diagram which is difficult to quantitatively evaluate for a specific range of flow parameters. The equation by Arita and Jirka [2,3] is semi-empirical and states the following equation to be solved:

$$\lambda_i = 0.076\left(1 - \frac{Ri}{\sqrt{Ri^2 + Ri_*^2}}\right) + \frac{2}{Re}\frac{z_1}{\delta_u}, \tag{29}$$

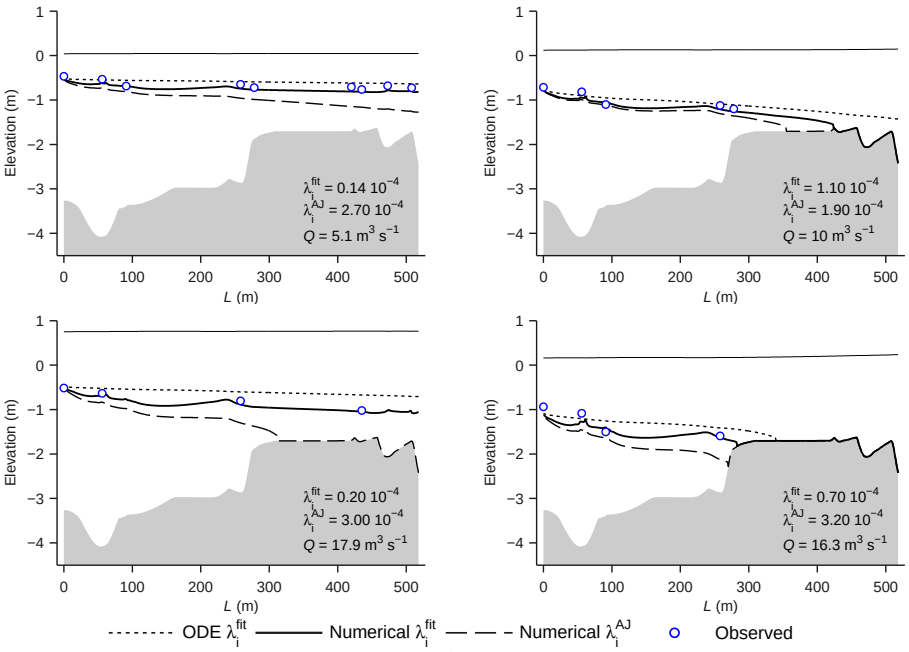

Fig. 8 Numerical solutions of the salt-wedge shape compared against field observations, for different freshwater flow rates Q. The solutions obtained by ODE (Eq. 26) are compared to the proposed numerical model (Eq. 22-25). Both λ_i^{fit} (fitted interfacial friction factor) and λ_i^{AJ} (computed from the Arita and Jirka model [2]) are considered.

with

$$\frac{\delta_u}{z_1} = \left(\frac{500}{Re}\right)^{1/2} + \frac{Ri_*}{\sqrt{Ri^2 + Ri_*^2}}\left[1 - \left(\frac{500}{Re}\right)^{1/2}\right], \tag{30}$$

where $Ri_* = 0.25$ is a critical Richardson number. Fig. 8 suggests that the model by Arita and Jirka [2] generally overestimates λ_i and the interface slope, and thus underestimates the salt-wedge intrusion length. Furthermore, the values of λ_i^{fit} obtained by fitting the numerical solutions to the observed data, and the values of λ_i^{AJ} obtained from Eq. (29) sometimes disagreed by an order of magnitude (Fig. 8), as will be shown in more details in the section 4. Sorgard [39] also found that the model by Arita and Jirka underestimated the salt-wedge length in the Glomma River estuary.

The results of fitting the numerical solutions to the observed data and the computed flow parameters are shown in Table 2. All of the following values are computed from the numerical solutions based on the assumption of zero interfacial layer thickness and they represent an along-wedge averaged values. The bed friction factor λ_b was obtained from Manning's equations with $n = 0.025$ s m$^{-1/3}$, and it ranged from 3.4×10^{-3} to 3.9×10^{-3}. Interfacial friction factor λ_i was fitted as previously described, and it ranged from 7.0×10^{-5} to 1.6×10^{-3}. The agreement between the computed and observed interface depth is quantified by *RMSE* (Eq. 28), and it showed a mean value of 0.11 m which is smaller that the mean value of the interfacial thickness $\bar{\delta}_i = 0.38$ m (Table 1). Velocity difference $\Delta u = u_1 - u_2$ ranged from 0.17 m s^{-1} to 0.47 m s^{-1}, where u_1 and u_2 are the upper and lower layer

Table 2 Fitted and computed data for the Rječina River estuary. Bed friction factor λ_b was obtained from Manning's equation with $n = 0.025$ s m$^{-1/3}$, interfacial friction factor λ_i was fitted to the observed data, $\Delta u = u_1 - u_2$, where u_1 and u_2 are the upper and lower layer velocity computed from $u = Q/A$ and averaged along the wedge, A was obtained from the computed salt-wedge shape and the channel geometry, shear velocity is $u_* = \sqrt{\tau_{int}/\rho}$, entrainment rate $E = w_e/\Delta u$, Reynolds number Re (Eq. 2), densimetric Froude number Fd (Eq. 3), bulk Richardson number Ri (Eq. 4), approximated gradient Richardson number Ri'_g (Eq. 8), and root mean square error $RMSE$ for agreement between the numerical solution and observed interface depth (Eq. 28)

nr.	$10^3\ \lambda_b$	$10^4\ \lambda_i$	$RMSE$ (m)	Δu (m s^{-1})	$10^3\ u_*$ (m s^{-1})	$10^4\ E$	$10^{-5}\ Re$	Fd	Ri	Ri'_g
1	3.4	1.0	0.05	0.17	1.7	0.59	0.6	0.54	3.9	3.6
2	3.5	0.7	0.05	0.20	1.6	0.50	0.7	0.56	3.6	1.4
3	3.7	4.0	0.07	0.22	4.4	1.25	1.3	0.53	4.1	1.6
4	3.7	1.2	0.11	0.23	2.5	0.66	1.2	0.56	3.6	1.5
5	3.7	1.4	0.08	0.24	2.8	0.94	1.3	0.55	3.7	1.4
6	3.7	2.0	0.14	0.24	3.4	1.13	1.4	0.56	3.7	1.0
7	3.7	1.8	0.10	0.25	3.2	1.58	1.6	0.56	3.6	1.7
8	3.5	2.0	0.03	0.27	3.8	1.69	1.8	0.56	3.6	1.9
9	3.8	11.0	0.07	0.28	9.3	0.96	2.4	0.53	4.5	0.7
10	3.8	6.0	0.09	0.29	7.1	1.98	2.5	0.56	3.9	0.7
11	3.8	7.5	0.07	0.31	8.4	1.27	2.6	0.57	3.9	0.9
12	3.6	9.5	0.13	0.30	9.0	1.35	2.5	0.53	4.3	0.8
13	3.6	6.0	0.07	0.33	7.9	1.39	2.9	0.60	3.5	0.7
14	3.6	5.0	0.07	0.34	7.5	1.29	2.9	0.62	3.3	0.5
15	3.6	10.5	0.15	0.33	10.6	2.03	3.0	0.56	4.1	0.9
16	3.7	4.0	0.15	0.34	6.7	2.17	3.2	0.57	3.6	0.7
17	3.6	7.0	0.12	0.37	9.6	2.53	3.8	0.61	3.3	0.9
18	3.6	13.0	0.11	0.37	13.2	2.13	3.7	0.59	3.7	1.5
19	3.6	6.0	0.12	0.36	8.8	2.29	3.7	0.59	3.6	1.0
20	3.6	2.0	0.04	0.37	5.2	1.33	3.7	0.60	3.3	0.6
21	3.9	11.0	0.36	0.47	15.3	5.56	6.2	0.64	3.7	0.7
22	3.8	16.0	0.30	0.44	17.7	6.19	6.3	0.61	4.1	0.8

average velocity, computed from $u_{1,2} = Q/A_{1,2}$, where upper layer A_1 and lower layer A_2 cross section area was obtained from the computed salt-wedge shape and digitalized channel geometry. Interfacial shear velocity is $u_* = \sqrt{\tau_{int}/\rho}$, ranging from 1.6×10^{-3} m s^{-1} to 17.7×10^{-3} m s^{-1}, and the entrainment rate is $E = w_e/\Delta u$, ranging from 0.5×10^{-4} to 6.2×10^{-4}. Nondimensional parameters showed the following values: Reynolds number $Re = 6\times10^4 - 6\times10^5$ (Eq. 2), densimetric Froude number $Fd = 0.53 - 0.64$ (Eq. 3), and bulk Richardson number $Ri = 3.3 - 4.5$ (Eq. 4). We additionally computed that an approximation of the Richardson gradient number Ri'_g (Eq. 9), which is more closely linked to the interfacial processes, ranged from 0.5 to 3.6.

4 Discussion

To better understand the hydrodynamic processes in this microtidal salt-wedge we present several figures (Fig. 9) to show how the governing parameters change with the freshwater flow rate. In general, as Q increases, salt-wedge length becomes shorter and the interface is positioned lower. Both average upper layer depth h_1 and velocity difference Δu increase with Q. Hence, Re also increases with Q (not shown in the figure). The correlation of h_1 and Δu with Q is non-linear and very strong ($R^2 = 0.98$). However, it seems that as a results of

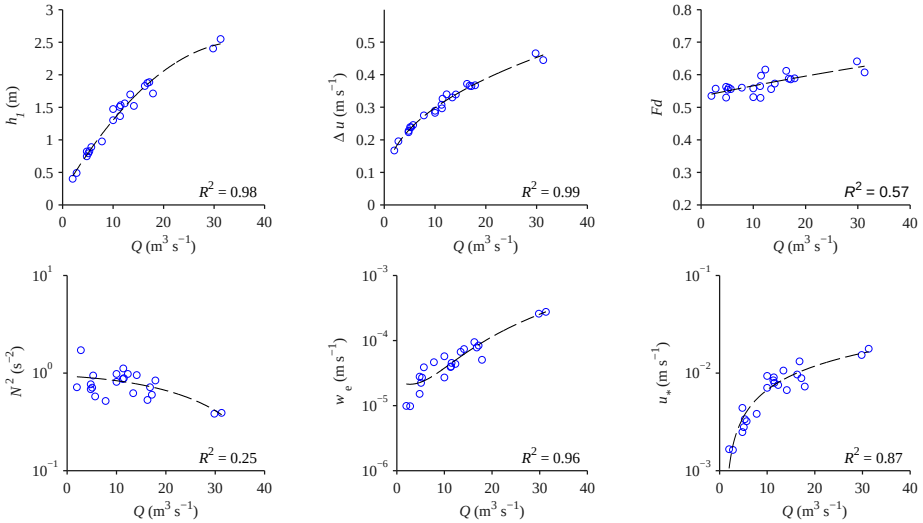

Fig. 9 Dependence of the upper layer depth h_1, velocity difference Δu, densimetric Froude number Fd, squared buoyancy frequency N^2, entrainment velocity w_e and interfacial shear velocity u_*, on the freshwater flow rate Q.

a sloped channel bed and different sea levels, Fd only slightly increases with Q; thus, the correlation in this case is relatively weaker ($R^2 = 0.57$).

In [16] typical values of N^2 where reported, ranging from 0.0025 to 0.01 s^{-2} for partially mixed estuaries, and up to 0.1 s^{-2} for salt-wedge estuaries. For example, in the Hudson River estuary, N^2 only occasionally reached a maximum of 0.1 s^{-2} [33]. Similar upper values were also found in other macrotidal salt-wedge estuaries, such as the Columbia River [23] and Snohomish River [46]. As described earlier, stratification strength estimated by N^2 in the Rječina River estuary shows values close to 1.0, confirming that microtidal salt-wedge estuaries may be characterized by much stronger stratification in comparison to the macrotidal salt-wedge estuaries, which is expected due to weaker tidal dynamics. Furthermore, it seems that N^2 decreases with increasing freshwater flow rate, although the correlation is not so strong ($R^2 = 0.25$), but the downward trend is noticeable.

In most salt-wedge estuaries, strong stratification and even the salt-wedge structure itself is maintained by high freshwater flow which dampens the vertical mixing caused by tidal motions [15]. In contrast, an increase of Q in microtidal salt-wedges may result in increased shear velocity at the interface which produces turbulent energy and increases vertical mixing [40]. The observations show that when the freshwater flow increases and the stratification is reduced (Fig. 9, lower left panel), and both w_e (Fig. 9, lower middle panel) and u_* (Fig. 9, lower right panel) increase with Q. On the other hand, for low Q, strong stratification reduces both interfacial shear and the entrainment. We should also note a very strong correlation of Q with w_e ($R^2 = 0.96$), as well as with u_* ($R^2 = 0.87$), which is surprising considering the complexity of turbulent processes in stratified environments, and a three-way interaction between stratification, shear and turbulent mixing. The strong correlation also justifies the numerous attempts to derive a suitable parametrization of these interfacial processes based on bulk flow parameters.

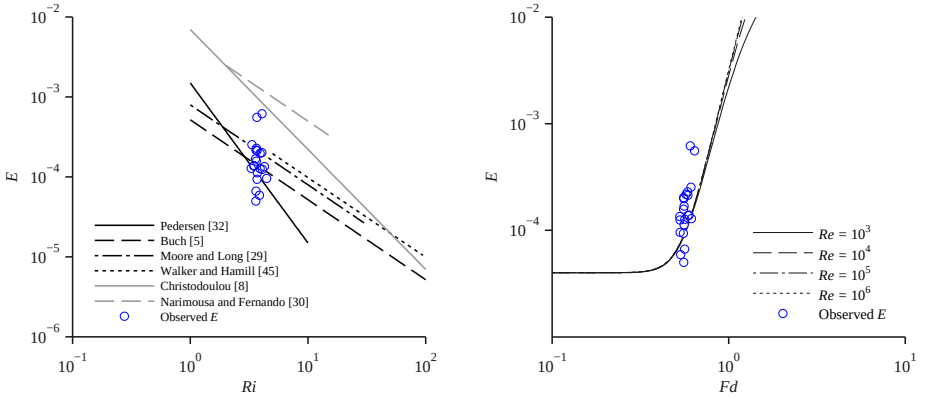

Fig. 10 Dependence of entrainment rate E on bulk Richardson number Ri (with comparison to several parametrisations) and densimetric Froude number Fd (with comparison to parametrisation [7])

4.1 Entrainment parametrization

Figure 10 shows the entrainment rate E plotted against the bulk Richardson number Ri and compared to several entrainment laws from the literature. Based on numerous experiments it is generally considered that E reduces with increasing Ri [5,8,29,30,32,45]. Surprisingly, in this case, Ri does not seem to be the main governing parameters for E; the data are in the expected range, but E shows a wide range of values, from 5×10^{-5} to 6×10^{-4}, for similar bulk Richardson number, $3.3 < Ri < 4.5$.

The most recent attempt to develop a new parametrization for entrainment can be found in [7]. Cenedese and Audduce recognized that in many numerical models for stratified flows, in particular overflows in straits and seas, the entrainment is parametrized using nondimensional bulk parameters averaged vertically and longitudinally. Based on laboratory and ocean data they derived a new empirical equation for the entrainment rate based on bulk parameters Fd and Re:

$$E = \frac{\min + AFd^{\alpha}}{1 + AC\,(Fd + Fd_0)^{\alpha}}, \tag{31}$$

where the best fit with the experimental and field data was found for $\min = 4\times10^{-5}$, $A = 3.4\times10^{-3}$, $Fd_0 = 0.51$, $\alpha = 7.18$, $B = 253.52$, and $C = f(Re)$. In Fig. 10 we also show the comparison of the observed E with Eq. (31). The agreement is not strong in this case either, but the values are in the expected range. Once more, the main difficulty is that the observations show a wide range of E for similar densimetric Froude number, $0.5 < Fd < 0.7$. However, according to Eq. (31) the entrainment rate is expected to increase over the same range as Fd increases from 0.44 to 0.77, which is relatively close to the computed values.

The scattering could be explained by the entrainment in estuaries possibly being intermittent and strongly influenced by local conditions [36]. One other possible explanation could be found in Strang and Fernando's study [41], where a considerable scattering was also observed for the range $3.2 < Ri < 5.8$. They found that as Ri increases from 3.2 to 5.8, interfacial instabilities gradually change from Kelvin-Helmholtz (K-H) waves to asymmetric Holmboe waves. The resonating K-H and Holmboe waves may be responsible for a wide disparity of entrainment rates. However, statements about the role of specific interfacial instabilities made solely on the range of bulk Richardson number is qualitative at best.

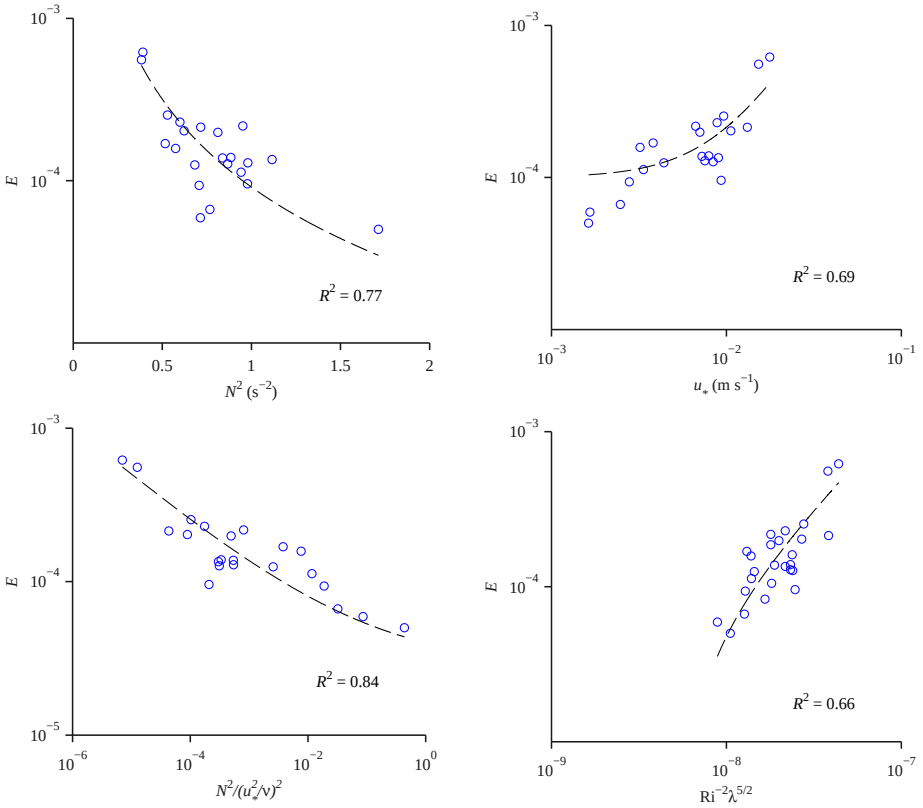

Fig. 11 Dependence of entrainment rate E on squared buoyancy frequency N^2, interfacial shear velocity u_*, the nondimensional ratio of stratification to shear $N^2/\left(u_*^2/\nu\right)^2$, and the combination of bulk Richardson number and interfacial friction factor $Ri^{-2}\lambda^{5/2}$, where $\lambda = (2\lambda_i + \lambda_b)/2$ is the average friction factor.

Both these comparisons suggest that the entrainment rate is difficult to accurately predict based on bulk flow parameters, such as Ri or Fd. Clearly, a more detailed local gradient measurements are needed to explain the mechanism of the observed entrainment processes.

To examine in more details the parameters that govern the entrainment processes, in Fig. 11 we show E plotted against buoyancy frequency N^2, interfacial shear velocity u_* and their non-dimensional ratio $N^2/\left(u_*^2/\nu\right)^2$. The latter parameter, although related to, should not be confused with the Richardson gradient number Ri_g (Eq. 8) which requires a detail measurement of the velocity profile, whereas, in this case the shear was only approximated by the interfacial shear velocity $u_*^2 = \lambda_i \Delta u^2$. We found that E is reduced with increasing stratification, and is intensified with increasing interfacial shear velocity, which is in agreement with other studies [40]. The dependence of E on the ratio of stratification to shear is very strong ($R^2 = 0.84$), suggesting that the entrainment may be predicted, more accurately, by the gradient, rather than bulk parameters.

However, we found that if the average friction factor, $\lambda = (2\lambda_i + \lambda_b)/2$, is combined with Ri, a satisfactory correlation may still be found between E and bulk parameters. Grubert [17, 18] found that shear stress should be included in entrainment parametrisations and suggested that the equations used for mixing in lakes and seas can be used, but with surface shear stress

replaced by a combination of bed and interfacial shear stress. Based on the experimental and field data, he proposed the following equation for the entrainment rate, $E = 2.4 Ri_*^{-3/2} Ri^{1/2}$, valid for $3.5 < Ri < 20$ [18]. Since, $Ri_* = Ri\lambda^{-1}$, we found a similar dependence of E on bulk parameters Ri and λ ($R^2 = 0.66$):

$$E \propto Ri^{-2}\lambda^{5/2} \tag{32}$$

This relation is shown in Fig. 11, and supports the conclusions by Grubert [18] that E is not a function of Ri alone, and that some form of shear stress should also be included. Clearly, the entrainment in arrested salt-wedges is mainly influenced by the shear stress at the interface and channel bed, which may be the main source of turbulent energy production. In comparison, for macrotidal salt-wedges it was found that during the ebb, the interfacial shear stress was the dominant source of turbulent mixing, while the shear stress at the channel bed was the main source of turbulent mixing during the flood [23]. Furthermore, the shear instabilities at the interface may even be the dominant mechanism for the initial breakdown of the salt-wedge structure [35, 46].

4.2 Interfacial friction parametrization

Currently, no consensus exists on which interfacial friction law should be applied for two-layer salt-wedge models, but the most frequently used is the one by Arita and Jirka [2]. In the study [2] a two-layer model was extended by including the entrainment and a new semi-empirical equation was proposed (Eq. 29), which consists of a laminar and turbulent contribution. The laminar contribution is dominant for low Re and suggests that λ_i decreases as Re increases, whereas the turbulent contribution is dominant for high Re and suggests that λ_i gradually becomes independent from Re and increases with Fd. However, the dependence of λ_i on governing parameters is difficult to quantify for the transition between the laminar and turbulent state. Furthermore, in [2] it was found that the stratified flow characterized by overall high Re numbers, may experience local laminarisation at the interface, which makes the efforts to derive a suitable parametrization even more complicated.

In Fig. 12 we show how λ_i relates to E, Fd, Re and how it agrees with the Arita and Jirka model (Eq. 29). The Arita and Jirka model is based on the assumption that the interfacial friction factor is directly linked to the entrainment rate, so that the following equality holds $\lambda_i = 2E$. The observed λ_i does indeed increase linearly with E; furthermore, it shows a very similar ratio $\lambda_i/E \approx 2.8$ as proposed in [2]. However, the discrepancies between the observed values and the Eq. (29) are noticeable. For the range of governing parameters considered here ($6 \times 10^4 < Re < 6 \times 10^5$ and $0.5 < Fd < 0.7$) we would expect λ_i to be confined to a more limited range of values ($5 \times 10^4 < \lambda_i < 8 \times 10^4$). Furthermore, λ_i should be independent from Re or slightly decrease with increasing Re. In contrast, the observed values of λ_i increase with $ReFd^2$ over a wide range, from 7.0×10^{-5} to 1.6×10^{-3}. However, it seems that the observed data are in the transitional region of the parameter space, for which the Eq. (29) is based only on empirical assumptions. When the dependence of λ_i on Fd is evaluated separately, we see a similar behaviour as for the entrainment rate; λ_i shows a wide range of values for very similar Fd. On the other hand, λ_i shows a positive correlation with Re ($R^2 = 0.62$).

In the search for a more suitable dependence of λ_i on bulk parameters, such as Re, Fd or Ri, we found the following empirical relationship, showing minimal scattering and the

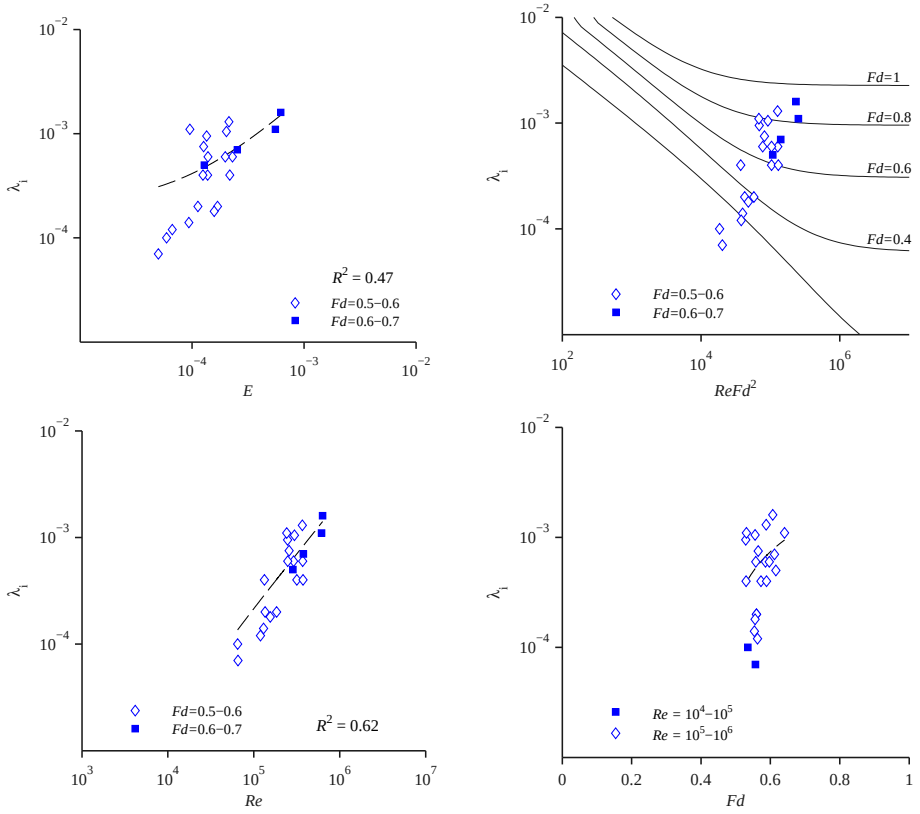

Fig. 12 Dependence of the interfacial friction factor λ_i on entrainment rate E, Re, Fd and on Keulegan number $ReFd^2$ with the Arita and Jirka equation [2] (solid lines for different Fd)

strongest correlation coefficient (see Fig. 13):

$$\lambda_i \propto \left(ReRi^3\right)^{0.9} \tag{33}$$

Although having high correlation ($R^2 = 0.82$) and a satisfactory predictive capacity for the salt-wedge in the Rječina River estuary, Eq. (33) is derived by curve fitting, and should be used with caution in other microtidal salt-wedges. A relatively high exponent for Ri could be explained by a very narrow range of Richardson numbers considered here. On the other hand, an increase of λ_i with Re is in contrast to previous studies [2, 9], and deserves additional discussion. Since ν is fairly constant in all considered observations, this dependence should primarily be seen as an increase of λ_i with Q, and consequently with both h_1 and Δu. It seems that interfacial processes in the Rječina River estuary, for the observed range of hydraulic conditions, exhibit the following pattern: as the freshwater flow rate increases, so does the upper layer velocity and the shear velocity at the interface which increases turbulent mixing; thus, interfacial layer thickness is increased and stratification is weakened (Fig. 9). However, it seems that the turbulent mixing also increases the apparent roughness at the interface, and hence we observe a positive correlation of λ_i with Re. This is only an assumption, and without direct observations of the velocity profile and the Reynolds stress we can not make any definite claims. There are, unfortunately, no similar field data sets available in

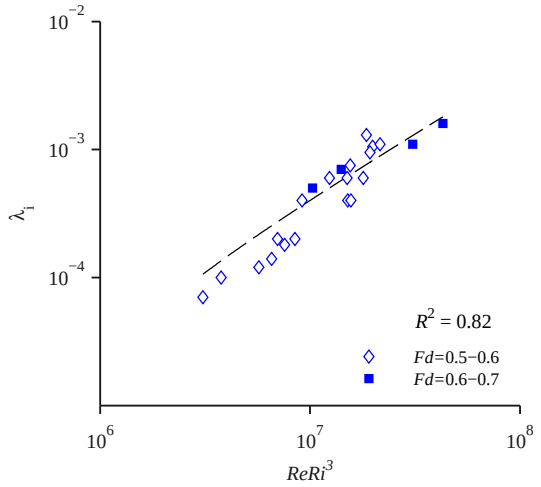

Fig. 13 Dependence of the interfacial friction factor λ_i on the combination of parameters $ReRi^3$

the literature, which are suitable for a comparison; only a few studies provided values for the interfacial friction factor, e.g., $\lambda_i = 1.6 \times 10^{-4}$ in the Glomma River [39] and $\lambda_i = 5 \times 10^{-4}$ in the Fraser River [28], and slightly higher $\lambda_i = 2 \times 10^{-3}$ in the Jadro River estuary [26]. However, these are only single values, lacking additional flow parameters, and are considered to be only average estimates for the interfacial friction factor. They do, however, fit inside the range of values observed in the Rječina River estuary.

The Eq. (33) can be further simplified by assuming that $R_1 \approx h_1$ and $u_2 \approx 0$, and also that r and ν are fairly constant for all observations, and thus do not have any significant explanatory power. Finally, we can write the following approximation $(ReRi^3)^{0.9} \sim (h_1/u_1)^4$. This simplification suggests that the interfacial friction factor in the Rječina River estuary increases with a ratio of the upper layer depth to the upper layer velocity.

5 Conclusion

The stratification, interfacial friction and entrainment in a microtidal salt-wedge estuary were studied through sampling campaigns at the Rječina River estuary over a two-year period. Based on a series of measured salinity and temperature profiles during different hydrographic conditions we estimated the strength of the stratification. The buoyancy frequency indicated that a highly stratified water column was present along the estuary for all considered flow rates. Maximum values of N^2 reaching up to 1.0, are amongst the highest ever reported in the literature from natural estuaries. In contrast to macrotidal salt-wedges it was shown that the stratification strength in the Rječina River estuary is reduced as the freshwater flow rate increases.

A simple two-layer box model was used to estimate the entrainment rate E. When E was plotted against Ri the scattering was significant for a relatively narrow range $3.3 < Ri < 4.5$. Further analysis revealed that E reduces with increased stratification, and increases with interfacial shear velocity. We found that E may be parametrized by bulk nondimensional parameters if the average friction factor (accounting for both bed and wall friction, as well

as the interfacial friction) is included, which is in accordance with previous studies (e.g., see [18]). In particular, the best fit was obtained when E was correlated with $Ri^{-2}\lambda^{5/2}$.

An improved two-layer steady numerical model was developed to predict the shape of the salt-wedge and estimate the interfacial friction factor λ_i by a fitting procedure. We extended the model [17], by considering the channel geometry with variable non-prismatic cross sections to accurately account for bed friction, lower layer dynamics, and entrainment. We showed that the proposed numerical model is an improvement on widely used ODE, or the analytical solution. Furthermore, none of the existing friction laws performed adequately for predicting the interfacial friction factor in Rječina Estuary. Contrary to previous assumptions, we found that in field conditions, λ_i may increase with Re for similar values of Ri. This is the first confirmation that in field conditions no quantitative similarity exists with laboratory experiments [21]. Hence, we propose a new equation (33), which agrees very well with the observed data. The biggest disadvantage of the proposed equation (33) is its entirely empirical nature. However, the involved parameters Re and Ri are supported by dimensional analysis and Eq. (33) can successfully describe the interfacial friction in the Rječina River estuary for a wide range of freshwater flow rates.

The results from this study emphasize the need for additional experiments at a sufficiently large scale or controlled observations in the field to reveal the details of interfacial processes in a salt-wedge estuary. Although we adopted a simple but widely used two-layer numerical model, the results agree very well with the field observations when λ_i and E are accurately estimated. Clearly, the relationship between λ_i and governing flow conditions is not sufficiently investigated for highly stratified conditions in the field. More detailed observations are needed, preferably direct measurements of both mean flow parameters and turbulent processes at the interface.

Also, one of the main assumptions in two-layer models is high density stratification along the wedge and negligible depth of the interfacial layer. As the observations show, this is only true for small to moderate Q in microtidal salt-wedges. For higher Q the stability is compromised and interfacial layer depth increases to a point where this initial assumption becomes questionable. Hence, in addition to detailed measurements, more advanced multilayer models are also needed to more adequately describe the salt-wedge dynamics.

Acknowledgements This work was supported by Ministry of Science, Education and Sports of the Republic of Croatia under the project number 114-0982709-2549 (Hydrology of Sensitive Water Resources in Karst) and under the project number RC.2.2.06-0001 (Research Infrastructure for Campus-based Laboratories at University of Rijeka), which was co-funded by the European Fund for Regional Development.

References

1. Abraham, G., Karelse, M., Van Os, A.: On the magnitude of interfacial shear of subcritical stratified flows in relation with interfacial stability. J Hydraul Res **17**(4), 273–287 (1979)
2. Arita, M., Jirka, G.H.: Two-layer model of saline wedge. I: Entrainment and interfacial friction. J Hydraul Eng **113**(10), 1229–1246 (1987)
3. Arita, M., Jirka, G.H.: Two-layer model of saline wedge. II: Prediction. J Hydraul Eng **113**(10), 1249–1263 (1987)
4. Balloffet, A., Borah, D.K.: Lower Mississippi Salinity Analysis. J Hydraul Eng **111**(2), 300–315 (1985). DOI 10.1061/(ASCE)0733-9429(1985)111:2(300)
5. Buch, E.: On entrainment observed in laboratory and field experiments. Tellus **34**, 307–311 (1982). DOI 10.3402/tellusa.v34i3.10815
6. Carstens, T.: Turbulent diffusion and entrainment in two-layer flow. Waterways Harbors Coast Eng Div **96**(1), 97–104 (1970)

7. Cenedese, C., Adduce, C.: A New Parameterization for Entrainment in Overflows. J Phys Oceanogr **40**(1), 1835–1850 (2010). DOI 10.1175/2010JPO4374.1
8. Christodoulou, G.: Interfacial mixing in stratified flows. J Hydraul Res **24**(2), 77–92 (1986)
9. Dermissis, V., Partheniades, E.: Dominant shear stresses in arrested saline wedges. J of Waterway Port Coast Ocean Eng **111**(4), 733–752 (1985)
10. Dyer, K.R.: Estuaries: a physical introduction. John Wiley & Sons, London (1973)
11. Farmer, H., Morgan, G.: The salt wedge. Coast Eng Proc **1**(3), 54–64 (1952)
12. Fernando, H.J.: Turbulent Mixing In Stratified Fluids. Annu Rev Fluid Mech **23**(1), 455–493 (1991). DOI 10.1146/annurev.fluid.23.1.455
13. Fofonoff, N., Millard, R.: Algorithms for computation of fundamental properties of seawater. UNESCO Technical papers in marine science **44**, 53 (1983)
14. Garrett, C.: Frictional processes in straits. Deep Res Part II Top Stud Oceanogr **51**(4-5), 393–410 (2004). DOI 10.1016/j.dsr2.2003.10.005
15. Geyer, W.R., Ralston, D.K.: The Dynamics of Strongly Stratified Estuaries. In: Treatise Estuar Coast Sci, vol. 2, pp. 37–52. Elsevier Inc. (2011). DOI 10.1016/B978-0-12-374711-2.00206-0
16. Geyer, W.R., Scully, M.E., Ralston, D.K.: Quantifying vertical mixing in estuaries. Environ Fluid Mech **8**(5-6), 495–509 (2008). DOI 10.1007/s10652-008-9107-2
17. Grubert, J.: Interfacial mixing in stratified channel flows. J Hydraul Eng **115**(7), 887 – 905 (1989)
18. Grubert, J.: Interfacial mixing in estuaries and fjords. J Hydraul Eng **116**(2), 176–195 (1990)
19. Hogg, A.J., Hallworth, M.a., Huppert, H.E.: On gravity currents driven by constant fluxes of saline and particle-laden fluid in the presence of a uniform flow. J Fluid Mech **539**(-1), 349 (2005). DOI 10.1017/S002211200500546X
20. Ibanez, C., Saldana, J., Prat, N.: A model to determine the advective circulation in a three layer, salt wedge estuary: application to the Ebre River estuary. Estuar Coast Shelf Sci **48**, 271–279 (1999)
21. Jirka, G.H.: Circulation in the salt wedge estuary. In: Residual Currents and Long-term Transport, vol. 38, pp. 223–237. Springer, New York (1990)
22. Karelse, M.: Momentum and mass transfer in stratified flows. Tech. Rep. December, Delft Hydraulics Laboratory (1974)
23. Kay, D.J., Jay, D.A.: Interfacial mixing in a highly stratified estuary 1. Characteristics of mixing. J Geophys Res **108**(C3), 1–15 (2003). DOI 10.1029/2000JC000252
24. Krvavica, N., Kožar, I., Travaš, V., Ožanić, N.: Numerical modelling of two-layer shallow water flow in microtidal salt-wedge estuaries: Finite volume solver and field validation. J Hydrol Hydromech DOI 10.1515/johh-2016-0039. In Press
25. Krvavica, N., Mofardin, B., Ruzic, I., Ozanic, N.: Measurement and analysis of salinization at the Rječina estuary. Gradevinar **64**(11), 923–933 (2012)
26. Ljubenkov, I.: Hydrodynamic modeling of stratified estuary: case study of the Jadro River (Croatia). J Hydrol Hydromech **63**(1), 29–37 (2015). DOI 10.1515/johh-2015-0001
27. Ljubenkov, I., Vranješ, M.: Numerical model of stratifed flow - case study of the Neretva riverbed salination (2004). Gradevinar **64**(2), 101–112 (2012)
28. MacDonald, D.G., Geyer, W.R.: Turbulent energy production and entrainment at a highly stratified estuarine front. J Geophys Res C Ocean **109**(5), 1–17 (2004). DOI 10.1029/2003JC002094
29. Moore, M., Long, R.: An experimental investigation of stratified shearing flow. J Fluid Mech **49**(4), 635–655 (1971)
30. Narimousa, S., Fernando, H.J.: On the sheared density interface of an entraining stratified fluid. J Fluid Mech **174**, 1–22 (1987). DOI 10.1017/S0022112087000016
31. Partch, E.N., Smith, J.D.: Time dependent mixing in a salt wedge estuary. Estuarine Coast Marine Sci **6**(1), 3–19 (1978). DOI 10.1016/0302-3524(78)90038-5
32. Pedersen, F.B.: A monograph on turbulent entrainment and friction in two-layer stratified flow. Institute of Hydrodynamics and Hydraulic Engineering, Technical University of Denmark (1980)
33. Peters, H.: Observations of Stratified Turbulent Mixing in an Estuary: Neap-to-spring Variations During High River Flow. Estuar Coast Shelf Sci **45**(1), 69–88 (1997). DOI 10.1006/ecss.1996.0180
34. Poggioli, A.R., Horner-Devine, A.R.: The Sensitivity of Salt Wedge Estuaries to Channel Geometry. J Phys Oceanogr **45**(12), 3169–3183 (2015). DOI 10.1175/JPO-D-14-0218.1
35. Ralston, D.K., Geyer, W.R., Lerczak, J.a.: Turbulent mixing in a strongly forced salt wedge estuary. J Geophys Res Ocean **115**(12), 1–19 (2010). DOI 10.1029/2009JC006061
36. Sargent, F.E., Jirka, G.H.: Experiments on saline wedge. J Hydraul Eng **113**(10), 1307–1323 (1987)
37. Schijf, J., Schönfeld, J.: Theoretical considerations on the motion of salt and fresh water. In: Proceedings of Minnesota International Hydraulics Convention, pp. 321–333 (1953)
38. Sorgard, E.: A numerical, three-layered, stationary salt wedge model. J Geophys Res **96**(C7), 12,739–12,754 (1991). DOI 10.1029/91JC00846

39. Sorgard, E., Martinsen, T., Aas, E.: Drag coefficient at a stationary salt wedge. J Geophys Res **95**(C5), 7337–7345 (1990). DOI 10.1029/JC095iC05p07337
40. Stacey, M.T., Rippeth, T.P., Nash, J.D.: Turbulence and Stratification in Estuaries and Coastal Seas. In: Treatise Estuar Coast Sci, vol. 2, pp. 9–36. Elsevier Inc. (2011). DOI 10.1016/B978-0-12-374711-2.00204-7
41. Strang, E., Fernando, H.J.: Entrainment and mixing in stratified shear flows. J Fluid Mech **428**, 349–386 (2001)
42. Szymkiewicz, R.: Numerical modeling in open channel hydraulics. Springer, London (2010)
43. Tamai, N.: Friction at the interface of two-layered flows. Coast Eng Proc **1**(15), 3169–3188 (1976)
44. Vreugdenhil, C.: Computation of gravity currents in estuaries. Ph.D. thesis, TU Delft (1970)
45. Walker, S., Hamill, G.: Temporal observations of interfacial layer between fluids of different density. J Waterway Port Coast Ocean Eng **125**(1), 20–28 (1999)
46. Wang, B., Giddings, S.N., Fringer, O.B., Gross, E.S., Fong, D.A., Monismith, S.G.: Modeling and understanding turbulent mixing in a macrotidal salt wedge estuary. J Geophys Res **116**(C2), 1–23 (2011). DOI 10.1029/2010JC006135